
Article:
Porter, C.P., Bezzina, J.P., Clegg, F. et al. (1 more author) (2017) Polymeric seal degradation in nuclear power plants: Determination of physical and mechanical properties. Journal of Applied Polymer Science. ISSN 0021-8995

https://doi.org/10.1002/app.45814

Polymeric Seal Degradation in Nuclear Power Plants: Determination of Physical and Mechanical Properties

Christopher P. Porter[a,b], James P. Bezzina[a], Francis Clegg[c], Mark D. Ogden[a]

[a]Department of Chemical and Biological Engineering, University of Sheffield, Portobello Street, Sheffield, S1 3JD.

[b]R S Bruce Metals and Machinery Ltd, March Street, Sheffield, S9 5DQ

[c]Materials and Engineering Research Institute, Sheffield Hallam University, City Campus, Howard Street, Sheffield, S1 1WB, U.K.

Main Author Correspondence: *m.d.ogden@sheffield.ac.uk*

ABSTRACT

To assess the suitability of different materials as polymeric seals in the Nuclear Industry three commercial samples of nitrile rubber at grades BA40, BA50 and BA60 have been tested. Differential Scanning Calorimetry (DSC) was used to find the glass transition temperature (T_g) and a Lloyds Texture Analyser 500 (TA500) was used to find the ratio of energy returned during relaxation against energy applied during compression. The mechanical properties determined from these experiments were then compared against the materials infrared (IR) spectra to infer structural characteristics. These were in turn cross-analysed against the materials ability to swell in a liquid solvent and absorption behaviour in a gaseous solvent. From this information a statement could be made about each material's capacity to perform as a seal. It was thus found that the high energy retention and low absorption characteristics of BA40 made this material the best choice out of those studied for use as a polymeric seal in the nuclear industry.

INTRODUCTION

Recent maintenance optimisation on Nuclear Power Plants (NPP) has resulted in the reassessment of component lifetimes and maintenance procedures. It is well established that previous lifetime assessments on polymeric seals used in the nuclear industry have been overly conservative and are therefore being reviewed.

For an effective seal the closing force applied from the component onto a boundary wall must exceed the sealed fluid pressure. The ability for a material to impart this closing force is therefore a function of their molecular structure and all external forces that are being applied. During compression of an elastomer the polymer chains will slide past one another and dissipate this energy. However, the presence of crosslinks prevents chain movement and retains this energy, acting back against the compression and creating a sealing force. Changes in the microstructure, following exposure to detrimental operational conditions, may therefore lead to degradation of the material's sealing capacity. It is clear from this that the behaviour under compression and relaxation are key factors in the materials ability to perform as a seal, as well as the gel-content and crosslink density of the molecular structure.

Nitrile rubber, NBR, is typically used as the base elastomer in the manufacture of dynamic seals as its acrylonitrile (ACN) content gives it excellent resistance to lubricating oils and grease [1]. There exists significant work in the characterisation of NBR rubber [2-3] and identification of its material properties [4-7], however, it is evident throughout these reports that the inclusion of a number of different additives, such as carbon black powder, fillers, vulcanising agents, anti-oxidants, etc., affect the elastomers overall material properties in

different ways. It is also clear that no attempt has been made to cross-analyse the microstructural characteristics inferred from these experiments to the materials absorption behaviour of both a liquid solvent and gaseous mixture and link the findings to the materials sealing capacity and ability to produce a pressure boundary. This work, therefore, assesses the glass transition temperature (T_g) and the mechanical compression behaviour of a set of three commercially available NBR samples and compares the findings against their characteristics assessed by IR, TGA and Dynamic Mechanical Analysis (DMA). A comparison is then drawn between these structural characteristics, the ability to swell in an appropriate liquid solvent and the absorption behaviour in an appropriate gaseous solvent. With an understanding of how the material responds in these environments a statement about its ability to function as a seal can then be made.

EXPERIMENTAL

Materials

Three NBR sheets at a thickness of 6 mm were obtained from Whitby and Chandler Ltd. at hardness grades BA40, BA50 and BA60 [8]. All samples are made from the same base elastomer, NBR, but will contain different quantities of ACN and butadiene (BDN), as well as a variety of additives and fillers. The types and quantities of these components are proprietary knowledge and as such are not detailed here.

Infra-red Spectroscopy

Approximately 4 mm thickness was removed from the surface of each sample before Fourier Transform IR Spectroscopy was carried out on a Perkin Elmer Frontier FTIR spectrometer with a diamond Attenuated Total Reflectance (ATR)

attachment. The spectroscopic analysis was performed between 4000 and 500 cm^{-1}, at a resolution of 4 cm^{-1} and with an accumulation of 4 scans.

Thermogravimetric Analysis

Between 5 and 20 mg of sample was placed in a ceramic crucible and analysed through thermogravimetric analysis using a Perkin Elmer TGA 4000 (balance precision of 0.01%), controlled by the Pyris™ software. The samples were subject to an increase from 40 to 150°C at a ramp rate of 50°C.min^{-1}, then held for 10 min before another increase to 900°C at a ramp rate of 50°C.min^{-1}. Once temperature was reached, it was held at 900°C for a further 10 min, to ensure total loss of organic component of rubber samples. All measurements were made in triplicate within N_2 and O_2.

Glass Transition Temperature

5 mg of sample was cut into as small as reasonably practicable monoliths and placed in a Perkin Elmer Diamond DSC to identify T_g. This was calculated at 63% along the transition onset to transition termination [9]. A temperature range from 213 to 293 K was assessed with a ramp rate of 10 K min^{-1}.

Mechanical Behaviour

A Lloyds TA500 Texture Analyser was used to compress 7 mm diameter cylindrical pellets of sample through a compression-relaxation programme at a movement rate of 1 mm min^{-1} carried out at 1, 2, 3, 4 and 5 mm set deflections. The trapezoidal rule, **Error! Reference source not found.**, was then used to calculate the integral of the compression and relaxation curves, the ratio of which was identified as the Retention Factor (RF), Equation 2, and used to determine the energy retention potential of the elastomeric microstructure.

$$\text{Integral area} = \int_a^b f(x)dx \approx (b-a)\left[\frac{f(a)+f(b)}{2}\right] \quad (1)$$

where *a* and *b* are two locations on the x axis.

$$\text{Retention Factor} = \frac{\int R}{\int C} \quad (2)$$

where R and C are the integrals of the relaxation and compression curves, respectively.

Dynamic Mechanical Analysis

A Perkin Elmer DMA 8000 was used to assess the storage modulus and tan delta (damping). The sample width, thickness and length were approximately 6.0 mm, 1.5 mm and 10.0 mm, respectively. Each sample was held in tension mode and heated from -100 to 100 °C at 3 °C/minute. Strain was modulated at 0.2 % and at a rate of 1 Hz.

Absorption Behaviour

Toluene

Toluene is typically used as a liquid solvent for organics and so was chosen as the liquid component for the absorption studies. The procedure set out in ASTM D6814 calculates the crosslink density of crumb rubber [10]. As the polymer-solvent interaction parameter is a function of both materials and the chemical make-up of the rubber is not known this calculation is not possible and so the procedure has been adapted in the following manner.

The samples were cut using a fresh, sharp blade on a Stanley Knife into approximately 6 mm^3 cubes and placed in approximately four sample-volumes of toluene and allowed to reach equilibrium over a period of 72 hours, changing the solvent for new every 24 hours. An AnD GR-202 micro balance with a

repeatability of 0.01 mg was used in conjunction with **Error! Reference source not found.** to calculate percentage increase in mass and a caliper with a repeatability of 0.01 mm was used in conjunction with **Error! Reference source not found.** to calculate percentage increase in volume.

$$\Delta_{M\%} = \frac{M_t - M_0}{M_0} x100 \quad (3)$$

$$\Delta_{V\%} = \frac{L_t W_t T_t - L_0 W_0 T_0}{L_0 W_0 T_0} x100 \quad (4)$$

where $\Delta_{M\%}$ is the percentage mass increase, M is the mass in g, $\Delta_{V\%}$ is the percentage volume increase, L, W and T are the length, width and thickness in m and the subscripts t and 0 denote final and initial times, respectively.

CO_2

CO_2 is used as a coolant in some NPPs and was therefore chosen as the gaseous component in the absorption studies. 50-100 mg of sample was dissected into approximately 1 mm^3 monoliths and placed into a Hiden Isochema Intelligent Gravimetric Analyser 002 (IGA-002). The samples were taken down to vacuum to remove any previously absorbed gases and then underwent 0.1 MPa pressure increments between 0.1 and 1 MPa with CO_2 under isothermal conditions. During equilibration the increase in mass was recorded and the kinetic data was fitted to the pseudo-first (PFO) and pseudo-second order (PSO) rate equations [11] shown in Table 1. The thermodynamic data was then fitted against the Freundlich (F) [12], Langmuir (L) [13], Temkin (T) [14] and Dubinin-Radushkevic (DR) [15] isothermal models. The five-error equation procedure as set out by *Ho, Porter and McKay* [16] was used to identify the Sum of the

Normalised Error (SNE) values and find the rate equations and isothermal models that best fit the experimental data.

Table 1: Kinetic Rate Equations and Isothermal Models

Model	Equation	
PFO	$q_t = q_e\left(1 - e^{-k_1 t}\right)$	(5)
PSO	$q_t = \frac{k_2 q_e^{\,2} t}{1 + k_2 q_e t}$	(6)
F	$q_e = a_F C_e^{\,1/n_F}$	(7)
L	$q_e = \frac{q_m a_L C_e}{1 + a_L C_e}$	(8)
T	$q_e = \frac{RT}{b_T} \ln\left(a_T C_e\right)$	(9)
DR	$q_e = q_D \exp\left\{ - B_D \left[RT \ln\left(1 + \frac{1}{C_e}\right)\right]^2 \right\}$	(10)

where q is the uptake of CO_2 in $kg \cdot kg^{-1}$ and the subscripts t, e and m denote the uptake at time t, at equilibrium and the maximum respectively, k_1 is the first order rate constant in s^{-1}, k_2 is the second order rate constant in $kg \cdot kg^{-1} \cdot s^{-1}$, t is the time in s, C_e is the concentration of the solute in the gas phase in $kg\ m^{-3}$, a_F and n_F are Freundlich Isotherm Constants, a_L is the Langmuir Isotherm Constant, R is the Universal Gas Constant in $J\ mol^{-1}\ K^{-1}$, T is the temperature in K, a_T and b_T are the Temkin Isotherm Constants and q_D and B_D are the Dubinin-Radushkevic Isotherm Constants.

RESULTS

Infra-red Spectroscopy

The three IR spectra can be seen in Figure 1. The typical triple peak seen in polymers between 3000 and 2800 cm^{-1} were evident (a-c) as well as a peak at

2235 cm^{-1} (d), indicative of the C≡N bond in NBR. A peak at 1720 cm^{-1} in BA40 and 1736 cm^{-1} in BA50 and BA60 (e) suggested the presence of carbonyl stretching, C=O.

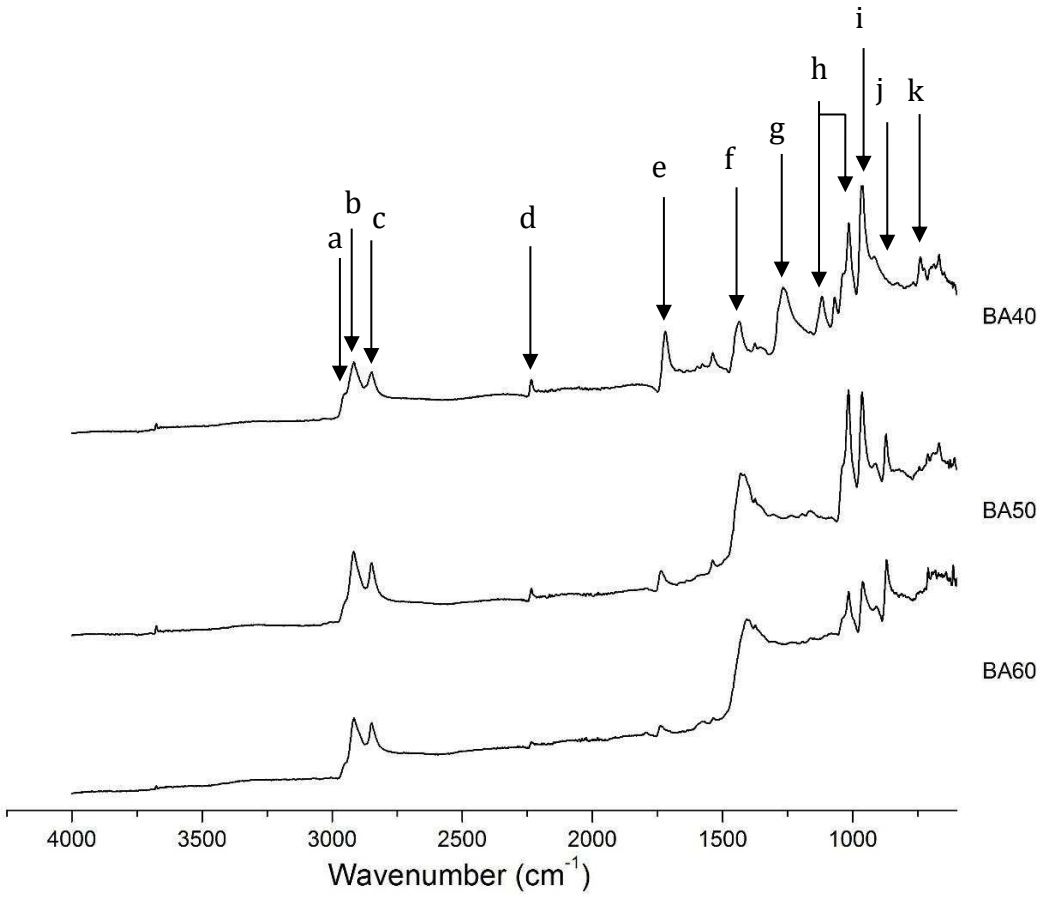

Figure 1: The IR Spectra for All Three Samples

The broad peak between 1436 and 1376 cm^{-1} (f) is typically linked to methylene vibrations on BDN that have been deformed due to the presence of C=O. The peaks at 964 and 741 cm^{-1} (i and k) were attributed to the *trans* and *cis* isomers of the C=C bond in BDN respectively, whilst the peak at 918 cm^{-1} (j) has been shown to correspond to the vinylidene bond, $RC=CH_2$. The remaining peaks were believed to correspond to the variety of additives found within the

elastomers. It can be seen from Fig. 1 that the "harder" the rubber, the spectral baseline rises, particularly at the right end. This could be associated with increasing carbon black content. This phenomenon occurs because carbon has absorbance throughout the entire infrared region and because, with the ATR method, light penetrates to a relatively large depth in the low wavenumber region.

Table 2: The Peaks Seen in the ATR-FTIR Spectra for all Three Samples Measured Between 3000 and 700 cm^{-1} and their Associated Bonds

Designation	Wavenumber (cm^{-1})	Associated Bond	Reference
a	2956	-CH stretching vibration of methylene groups	[17]
b	2918	assymetric stretching vibration of CH_2 in methylene (BDN units)	[6, 17-18]
c	2848	symmetric stretching vibration of CH_2 in methylene (ACN units)	[6, 17-20]
d	2235	-C≡N Nitrile	[4, 6, 18-19, 21-22]
e	1736 and 1720	carbonyl stretching of oxygen containing functional groups – linked to oxidation and crosslinks	[5-6, 19, 23-24]
f	1436-1376	bending vibration of CH_2 deformation due to C=O	[4, 6, 18, 20, 25-26]
g	1267	-C-N stretch	[5]
h	1117-1015	additives	[6, 27]
i	964 and 918	C=C transvinylidene – linked to BDN content	[2, 4-5, 18, 20, 25]
j	872 and 870	artefact of N containing functional group	[28-29]
k	741	cis configuration of C=C in BDN	[2, 4-5, 18, 20, 25]

Thermogravimetric Analysis

With increasing hardness a lower amount of weight was lost during TGA in a nitrogen atmosphere (at 550°C). However, following a switch to oxygen, the

BA50 sample has the largest amount of remaining weight, followed by the BA60 sample whilst the BA40 sample was fully decomposed, Table 3 and Figure 2.

Table 3: Weight Loss During Thermogravimetric Analysis

Sample	Weight Lost in N_2 (%)	Additional Weight Lost in O_2 (%)
BA40	82.0	18.0
BA50	71.7	24.5
BA60	63.6	33.7

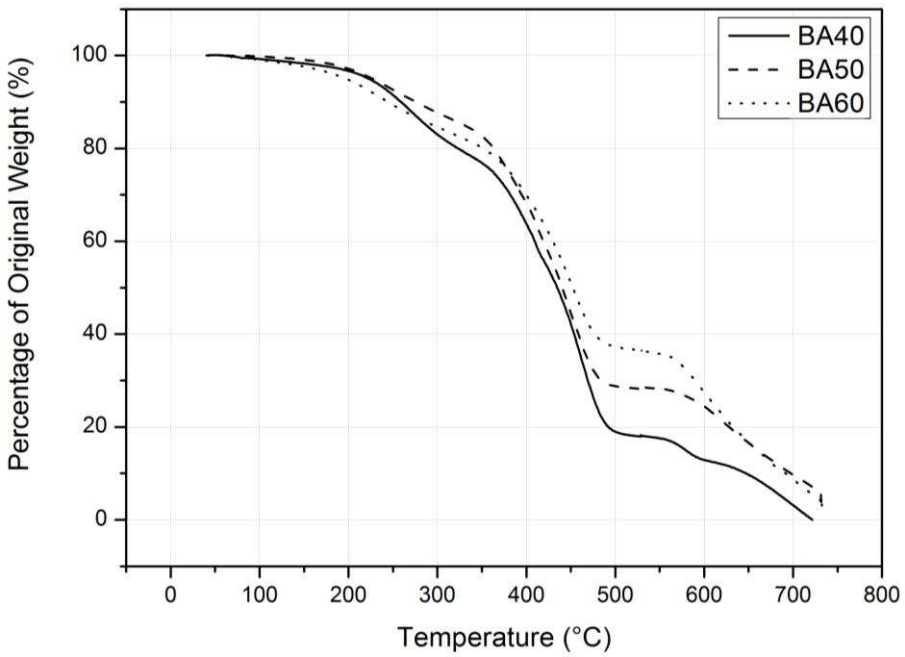

Figure 2: Thermogravimetric Results for All Three Samples

Material Properties

With increasing hardness RF showed a decreasing trend, Table 3, whilst BA40 had a slightly higher T_g but BA50 and BA60 were similar. As anticipated the storage modulus increased (more significantly between -10 to 100°C with increasing hardness (Figure 3), whilst the tan delta onset and maxima decreased with increasing hardness (Figure 4).

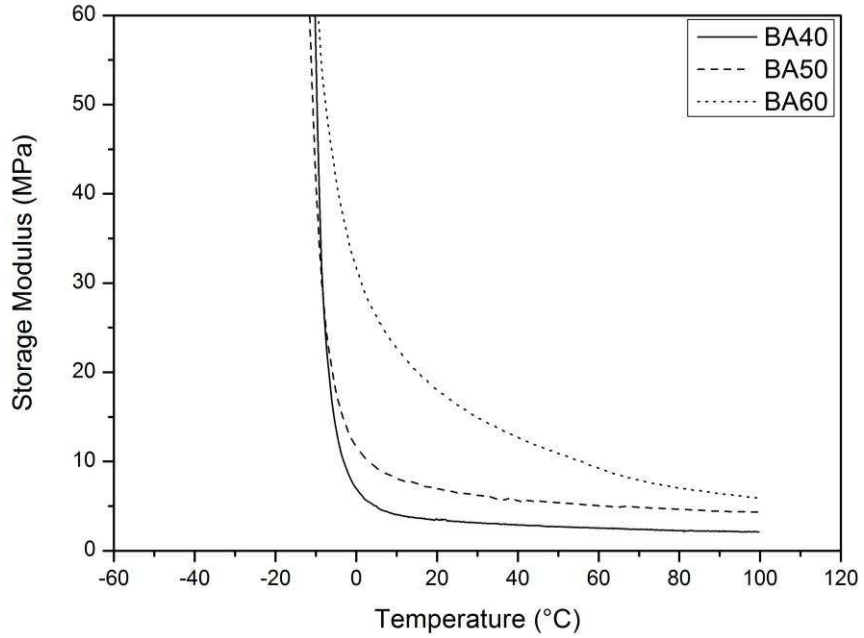

Figure 3: Storage Modulus Data for All Three Commercial Samples

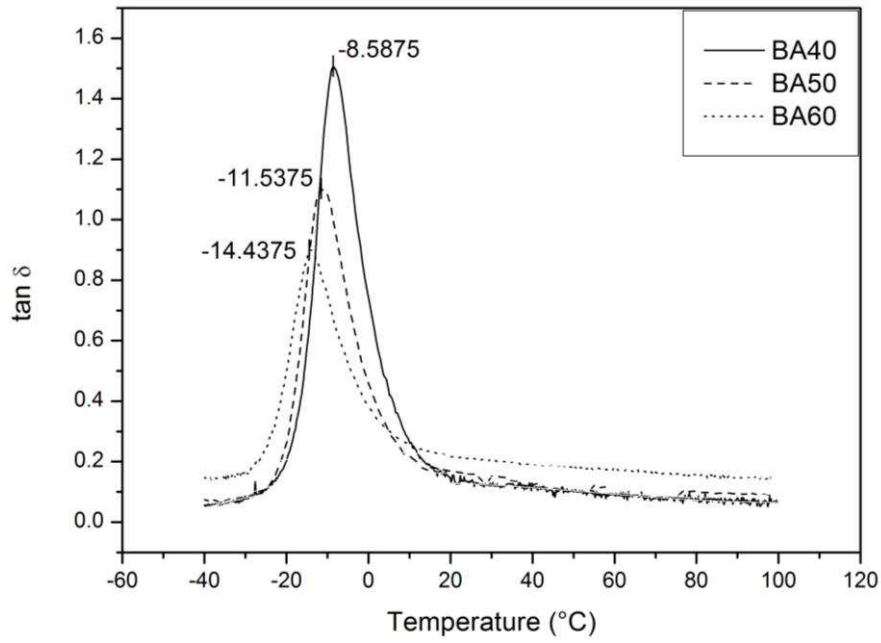

Figure 4: Tan Delta Data for All Three Commercial Samples Including the Calculated Peak Positions

Table 4: Material Properties for All Three Commercial Samples

Sample	T_g (°C)	RF	$Tan\ \delta\ Position$ (°C)	$Tan\ \delta\ Onset$ (°C)
BA40	-25.3 ± 0.3	0.834 ± 0.0092	-8.6	-25
BA50	-27.8 ± 0.4	0.711 ± 0.0040	-11.5	-28
BA60	-28.2 ± 0.4	0.515 ± 0.0035	-14.4	-28

Absorption Behaviour

Toluene

BA50 had the highest values for both $\Delta_{M\%}$ and $\Delta_{V\%}$ whilst BA40 had the lowest (Table 5). A difficulty arose in measurement of sample volume following absorption due to the increased compressibility of the samples.

Table 5: Percentage Mass and Volume Increase Following Swelling in Toluene for 72 Hours

Sample	$\Delta_{M\%}$	$\Delta_{V\%}$
BA40	89.1 ± 0.3	90 ± 10
BA50	135 ± 3	146 ± 3
BA60	108 ± 2	140 ± 10

CO_2 Kinetics

The kinetic models for CO absorption behaviour are given in Figure 5. The PFO model showed a better fit to the kinetic data for BA40, however the PSO model was best for both BA50 and BA60, Figure 5. The error margins in observable rate constants suggest the PSO model was the best kinetic model and showed an increasing trend with increasing hardness, a similar trend to that seen in the PFO model, Table 6.

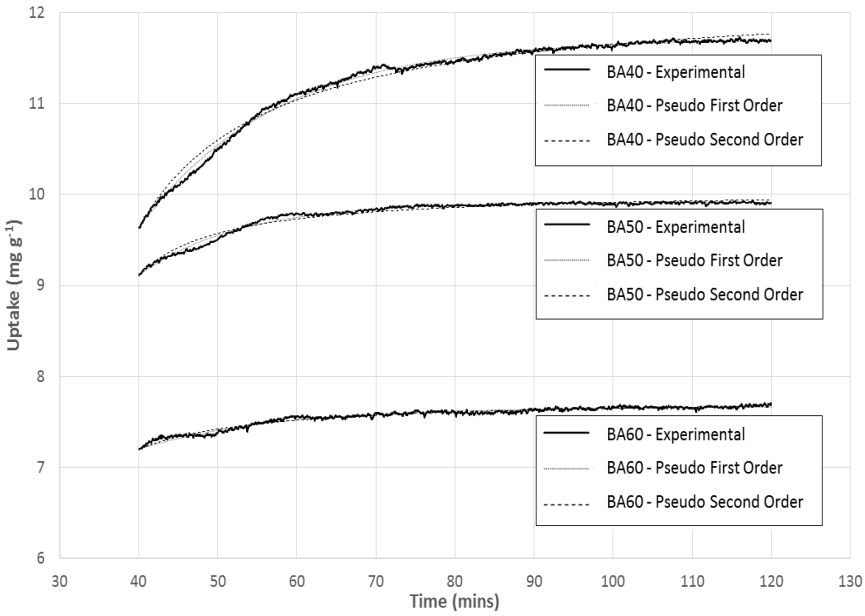

Figure 5: PFO and PSO Models Fitted to the Kinetic Data for BA40, BA50 and BA60 Measured in 0.5 MPa CO_2 at 20 °C

Table 6: The Observed Rate Constants for both the PFO and PSO Model Measured at 0.5 MPa CO_2 at 20 °C

Sample	$k_1(s^{-1})$	$k_2(kg\ kg^{-1}\ s^{-1})$
BA40	0.0561 ± 0.0003	0.792 ± 0.002
BA50	0.129 ± 0.003	2.69 ± 0.001
BA60	0.204 ± 0.005	5.35 ± 0.05

CO_2 Thermodynamics

During the thermodynamic assessment the Langmuir model did not converge on any parameter values. The Freundlich model showed the best fit for all samples tested and the resultant parameters suggested BA50 to have a higher absorption potential, Table 7 and Figures 6-8.

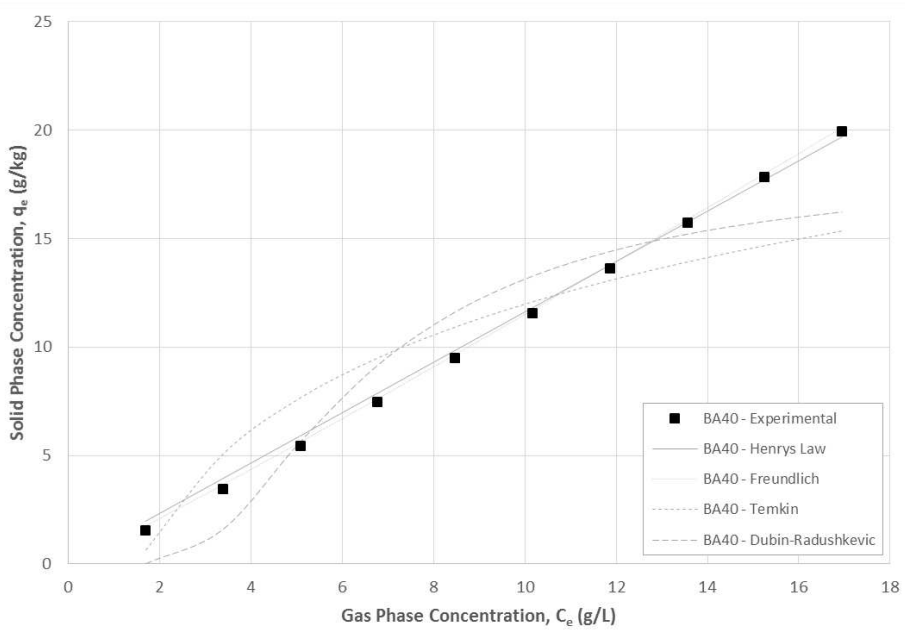

Figure 6: Isotherm Model Fits to the Thermodynamic Data for BA40 Measured Between 0.1 and 1 MPa CO_2 at 20 °C

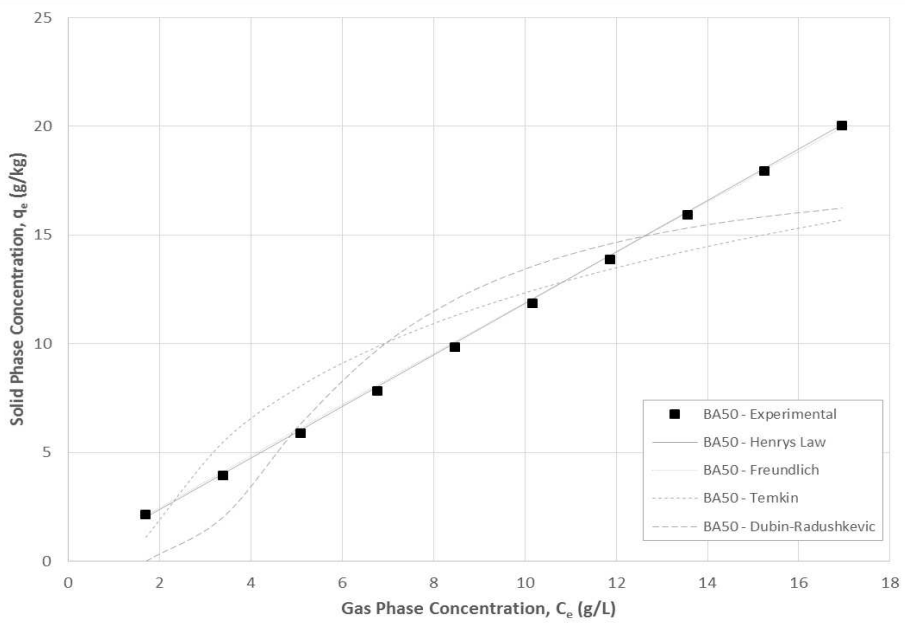

Figure 7: Isotherm Model Fits to the Thermodynamic Data for BA50 Measured Between 0.1 and 1 MPa CO_2 at 20 °C

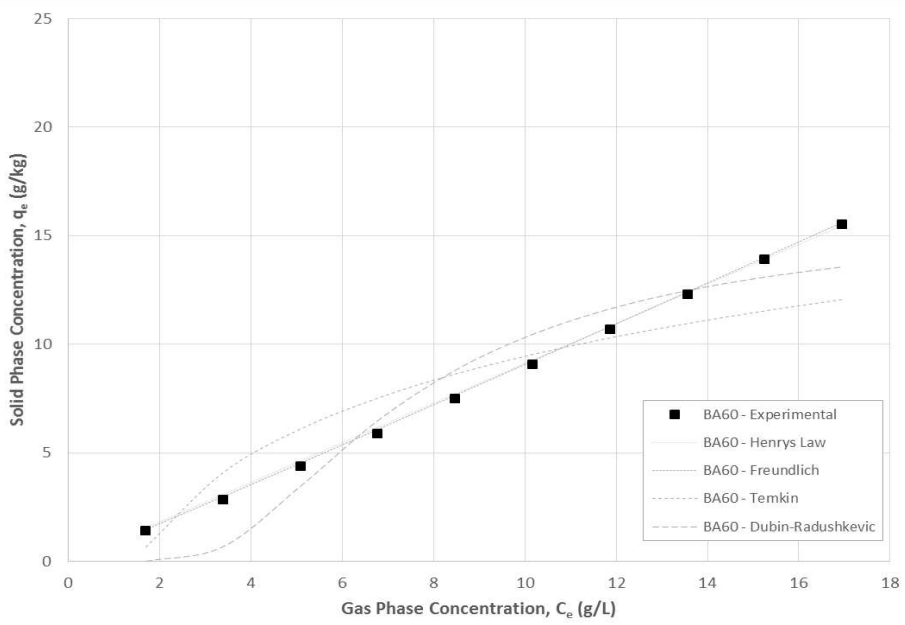

Figure 8: Isotherm Model Fits to the Thermodynamic Data for BA60 Measured Between 0.1 and 1 MPa CO_2 at 20 °C

Table 7: The Thermodynamic Data for All Three Commercial Samples Measured in CO_2 between 0.1 and 1 MPa at 20 °C

Isotherm Model	Parameter	BA40	BA50	BA60
Freundlich	a_F	1.00 ± 0.04	1.25 ± 0.03	0.85 ± 0.01
	n_F	0.94 ± 0.01	1.02 ± 0.01	0.972 ± 0.003
Temkin	b_T	382 ± 81	384 ± 78	492 ± 104
	a_T	0.66 ± 0.29	0.70 ± 0.31	0.67 ± 0.30
Dubinin-Radushkevic	$B_D(x\ 10^{-6})$	6.1 ± 1.7	5.5 ± 1.5	7.9 ± 2.4
	q_D	18 ± 19	18 ± 17	16 ± 29

DISCUSSION

Infra-red Spectroscopy

The C=O peaks at 1736-1720 cm^{-1} suggested the formation of crosslinks in the imide position [5-6, 19] during the manufacturing process as well as the presence of ester-containing additives, which also explained the shift in position

seen in the BDN-methylene vibrations between 1436 and 1376 cm^{-1}. All other noticeable and attributable peaks were typical of NBR and its monomers.

All peaks showed a similar diminished height to those seen by *Seehra, Yalamanchi and Singh* [4], who attributed the phenomena to the additives and fillers affecting the bond vibrations. This eliminated the potential for calculation of absolute quantities through peak heights. This is further supported by the increase in baseline in the low wavenumber region and the shift in the C=C-H out-of-plane bending vibration (trans-vinylene group) of polybutadiene that is representative of NBR at 964 cm^{-1} and 918 cm^{-1} which can be attributed to an increasing carbon black content of the rubber.

Thermogravimetric Analysis

The first negative derivative of the results, Figure 9, better show the trends between the data. It can be seen that the BA40 sample exhibits a peak at approximately 270°C that the other samples do not, the peak at approximately 460°C decreases with increasing hardness and that the peak after the switch to oxygen (approximately 530°C) increases with increasing hardness. The increased mass loss at 270°C for the BA40 sample suggests that it contains more additive or plasticiser (typically oils) than the other samples and that the carbon black content, as indicated by the weight remaining at 550°C, increases with increasing hardness.

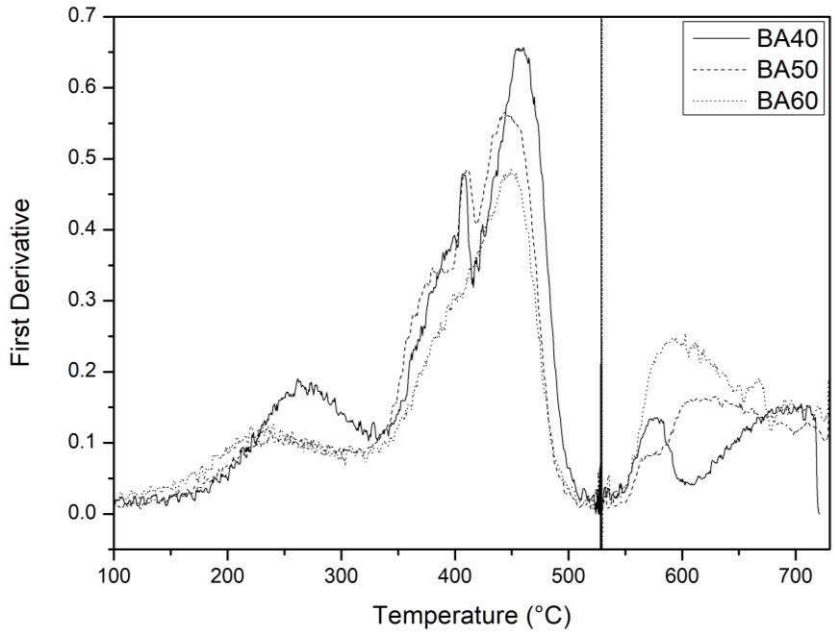

Figure 9: First negative derivative of the thermogravimetric analysis for all three Samples between 100 and 750 °C

Material Properties

The onset temperature of the tan delta maxima obtained by DMA shows a good match to the T_g values obtained by DSC again showing that T_g decreases with increasing hardness. In this work T_g showed only a 3 °C difference across all samples suggesting that the combined effect of both gel content and crosslink density within all samples was similar. This range of T_g values would suggest an ACN content of approximately 25-30% [30] however, many studies have shown that the additives and inclusions can have significant effect on the T_g values and thus this estimate would be susceptible to substantial error [31].

The compression curves produced during the mechanical testing regime were in good agreement with the literature [31], Figure 10, compressive stress-strain curves for NBR vulcanization filled with different CB concentration loadings.

From the data presented it could be inferred that the current BA samples tested could have a carbon black content <20%.

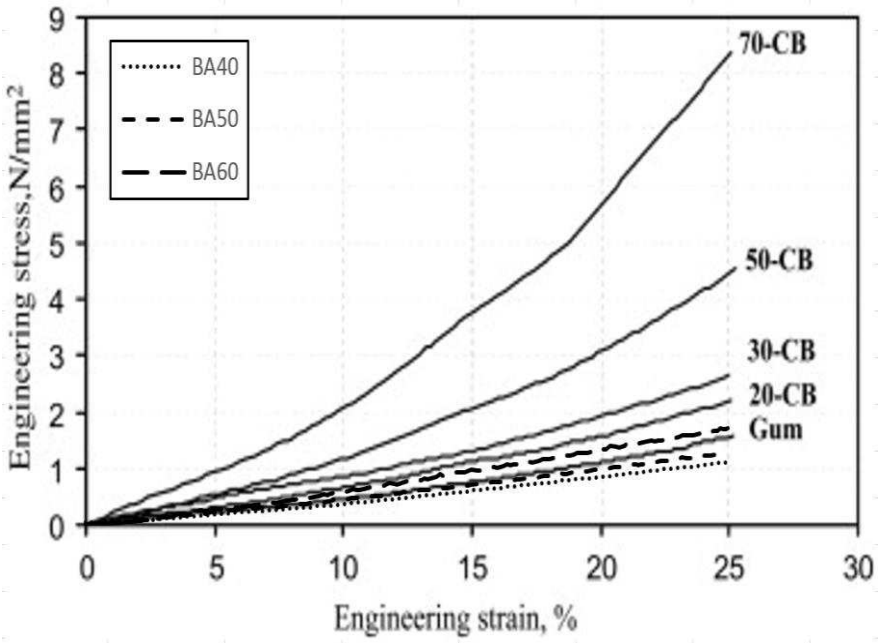

Figure 10: A Comparison of the Mechanical Compression Data for All Three Samples (dashed lines) against those NBR with increasing CB content found in the Literature [31] (solid lines)

RF is a numerical representation of the ability of the microstructure to retain the energy that has been applied through compression, due to the presence of crosslinks preventing energy dissipation through chain motion. However, this method only considers the rapid recovery mechanism, which has been linked to the local-scale readjustments of molecular order, [7]. The higher RF for BA40 therefore suggested lower local-scale chain mobility with a decreasing trend against increasing BA rating.

Absorption Behaviour

Toluene

The $\Delta_{M\%}$ values are in fairly good agreement with those found in the literature, [4]. The ratio of percentage mass to percentage volume increase suggested that the toluene filled the voids within the microstructure of the elastomer before expansion took place, Figure .

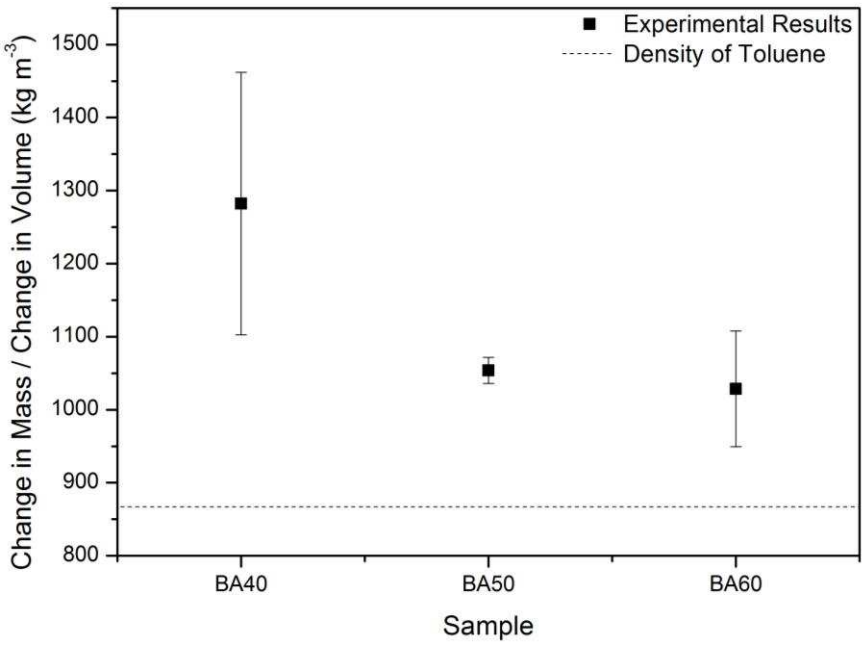

Figure 11: Change in Mass Divided by Change in Volume Against BA Hardness Rating

Although the margin of error is large, there was an apparent trend between ratio of mass to volume for absorbed toluene and T_g, suggesting that the softer samples provided more voids in which the toluene molecules could locate. As mentioned previously the $\Delta_{M\%}$ values showed no trend with increasing hardness. The larger swelling capacity seen in BA50 suggested a lower gel fraction as the chains had an increased capability to expand in the presence of an absorbing medium.

CO_2

Kinetics

The increasing tendency towards PSO kinetics over PFO kinetics with increasing hardness seen in Figure 5 is interesting. The kinetic data found by *George* [32] for absorption of CO_2 into a nitrile elastomer were fitted to a PFO model, however the obtained constants and any attempt at fitting to other models were not included in the report and so a comparison could not be made.

The increased observable rate constants for the harder samples suggested an increased affinity to the non-polar CO_2 molecule. Assuming 'like dissolves like' then this would suggest the harder samples have a higher proportion of the non-polar BDN pendant, suggesting that the typical method of increasing ACN content to increase hardness was not used and instead alternative additives were utilised. This may be linked to the evidence of decreasing void space in the harder samples as shown above.

Thermodynamics

The thermodynamic data for all samples was fairly linear between 0.1 and 1 MPa CO_2, in agreement with *George* [32], *Briscoe and Zakaria* [33] and *Fleming and Koros* [34]. This meant that during the fitting stage the Langmuir model could not predict the beginning of the saturation point and therefore could not converge on acceptable parameters (Figs. 6-8). The data showed the best fit with the Freundlich model, where a_F determines the slope of the line and n_F determines its curvature. The higher a_F for BA50 therefore suggested a greater absorption potential in this sample than in the others, whilst all n_F parameters were close enough to 1 to be considered linear and thus limited interaction between the absorbing molecule and the adsorbent existed.

Cross-comparison

The similar T_g between all samples and the slightly larger absorption capacities in both toluene and CO_2 seen in BA50 suggest that all samples have a similar crosslink density whilst the gel network of BA50 is somewhat smaller. One possible explanation for the anomalous behaviour of BA50 is crosslink clustering, as explained by *Vijayabaskar, Tikku and Bhowmick* [6], that increases the crosslink density but due to their localisation they do not incorporate many different polymer chains and thus the gel network does not show a corresponding increase. *Vijayabaskar, Tikku and Bhowmick* saw an increase in the proclivity for crosslink clustering in samples with higher BDN:ACN ratios and thus this clustering phenomena has been attributed to the BDN content of the samples.

CONCLUSIONS

Three commercial samples of nitrile rubber at grades BA40, BA50 and BA60 have been characterised by their IR spectra, T_g, RF and toluene and CO_2 absorption behaviour. The spread of T_g values suggested similar crosslink density between all samples whilst the slightly larger absorption capacities in both toluene and CO_2 for BA50 suggested that this sample had a slightly lower gel content, indicating the formation of crosslink clusters.

The IR spectra showed a similar vibration interference seen in the literature, however a number of peaks were visible if at a somewhat reduced intensity. The C≡N bond indicative of NBR was evident as was the C=O bond suggesting the formation of imide crosslinks and ester-containing additives. A number of peaks were evident only in BA40 and were thus attributable to unique additives and fillers that, without further investigation, were unidentifiable in this work.

Out of the available commercial samples, BA40 appeared to have the best physical and mechanical properties that would contribute to producing a good sealing material. The high RF means that a larger portion of the applied energy can be used in creating the sealing force, the low $\Delta_{M\%}$ means that the effects of increased friction found during absorption of lubricants into the material is reduced and the high T_g means that a greater portion of the polymer chains are already bound into the gel-network thus hindering the leaching of un-bound polymer chains into an active agent, such as grease or CO_2. In terms of behaviour in an NPP this sample would therefore produce a stronger seal with lower initial compression reducing the mechanical stress it is under and would also be less susceptible to expansion through exposure to grease and CO_2. The reduced expansion would prevent additional friction damage from the reciprocal movements expected in a dynamic seal.

ACKNOWLEDGEMENTS

The authors would like to thank EDF Energy for the financial support that permitted this work and the technical assistance offered by George Dowson and Ben Palmer of the University of Sheffield.

REFERENCES

1. S. Datta, Synthetic Elastomers, Rubber Technologists Handbook, J. R. White and A. K. De (Editors), 1 (2001) 47-74.
2. S. Chakraborty, S. Bandyopadhyay, R. Ameta, R. Mukhopadhyay and A. S. Deuri, Application of FTIR characterisation of acrylonitrile-butadiene rubber (nitrile rubber), Polym. Test., 26 (2007) 38-41.
3. P. Kusch, Identification of organic additives in nitrile rubber material by pyrolysis-GC-MS, LCGC North America, 31(3) (2013) 248-254.

4. M. S. Seehra, M. Yalamanchi, V. Singh, Structural characteristics and swelling mechanism of two commercial nitrile-butadiene elastomers in various fluids, Polym. Test. 31(4) (2012) 564-571
5. M. M. Hassan, R. O. Aly, A. H. El-Ghandour, H. A. Abdelnaby, Effect of gamma irradiation on some properties of reclaimed rubber/nitrile-butadiene rubber blend and its swelling in motor and brake oils, J. of Elastom. and Plast. 45(1) (2013) 77-94
6. A. V. Vijayabaskar, V. K. Tikku, A. K. Bhowmick, Electron beam modification and crosslinking: Influence of nitrile and carboxyl contents and level of unsaturation on structure and properties of nitrile rubber, Radiat. Phys. and Chem. 75 (2006) 779-792
7. A. Mostafa, A. Abouel-Kasem, M. R. Bayoumi, M. G. El-Sebaie, On the influence of CB loading on the creep and relaxation behaviour of SBR and NBR rubber vulcanizates, Mater. and Des. 30(7) (2009) 2721-2725
8. Whitby and Chandler Ltd., Rubber Sheets and Rubber Components [Available at http://whitby-chandler.co.uk/rubber-sheets-and-rubber-components.asp. Last Accessed: 18 January 2016].
9. Colby College, "Differential Scanning Calorimetry; First and Second Order Transitions in Polymers," [Online]. Available: http://www.colby.edu/chemistry/PChem/lab/DiffScanningCal.pdf. [Accessed 09 February 2016].
10. ASTM International, ASTM D6814: Standard test method for determination of percent devulcanisation of crumb rubber based on crosslink density, 2013

11. Y. S. Ho and G. McKay, A comparison of chemisorption kinetic models applied to pollutant removal on various sorbents, Process Saf. and Environ. Prot. 76(4) (1998) 332-340
12. H. M. F. Freundlich, Over the adsorption in solution, J. of Phys. Chem. 57 (1906) 385-470
13. I. Langmuir, The constitution and fundamental properties of solids and liquids. Part I: Solids, J. of the Am. Chem. Soc., 38(11) (1916) 2221-2295
14. C. Aharoni, M. Ungarish, Kinetics of activated chemisorption. Part II: Theoretical models, J. of the Chem. Soc. 73 (1977) 456-464
15. M. M. Dubinin, The potential theory of adsorption of gases and vapors for adsorbents with energetically nonuniform surfaces, Chem. Rev. 60(2) (1960) 235-241
16. Y. S. Ho, J. F. Porter, G. McKay, Equilibrium isotherm studies for the sorption of divalent metal ions onto peat: Copper, nickel and lead single component systems, Water, Air and Soil Pollut. 141(1) (2002) 1-33
17. V. Vijayabaskar and A. K. Bhowmick, Electron-beam modification of nitrile rubber in the presence of polyfunctional monomers, *J. of Appl. Polym. Sci.* 95(2) (2005) 435-447.
18. H. Fujiwara, J. Yamabe and S. Nishimura, Evaluation of the change in chemical structure of acrylonitrile butadiene rubber after high-pressure hydrogen exposure, *International J. of Hydrogen Energy,* 37(10) (2012) 8729-8733.
19. D. Tuyet-Trinh, M. Celina and P. M. Fredericks, Attenuated total reflectance infrared microspectroscopy of aged carbon-filled rubbers, *Polym. Degradation and Stability,* 77(3) (2002) 417-422.

20. F. Cardona, D. J. T. Hill, P. J. Pomery and A. K. Whittaker, “A comparative study of the effects of UV- and γ-radiation on copolymers of acrylonitrile/butadiene,” *Polymer International,* vol. 48, no. 10, pp. 985-992, 1999.
21. F. O'Keefe, “Identification of polymers by IR spectroscopy,” *Rubber World,* vol. 230, no. 3, pp. 27-37, 2004.
22. R. Parker and W. H. Waddell, “Quantitative Characterization of Polymer Structure by Photoacoustic Fourier Transform Infrared Spectroscopy,” *Journal of Elastomers and Plastics,* vol. 28, no. 2, pp. 140-160, 1996.
23. W. West, Chemical Applications of Spectroscopy, London: Wiley and Sons Ltd, 1956.
24. J. Bellamy, Advances in Infrared Group Frequencies, Moscow: Mir, 1971.
25. H. M. Abou Zied, Z. I. Ali, T. M. Abdel Maksoud and R. M. Khafagy, “Structure-property behaviour of polyethylene exposed to different types of radiation,” *Journal of Applied Polymer Science,* vol. 75, no. 2, pp. 179-200, 2000.
26. T. Yasin, Y. Nho, S. Khan and R. Ahmad, “Effect of polyfunctional monomers on properties of radiation crosslinked EPDM/waste tire dust blend,” *Radiation Physics and Chemistry,* vol. 81, no. 4, pp. 421-425, 2012.
27. J. Coates, “Interpretation of infrared spectra: A practical approach,” in *Encyclopedia of analytical chemistry*, Chichester, John Wiley and Sons Ltd., 2000.
28. J. Mohan, Organic Spectroscopy: Principles and Applications, 2 ed., Alpha Science International Ltd, 2004.

29. G. Helmchen, Houben-Weyl Methods of Organic Chemistry: v.b, 4 ed., Thieme Medical Publishers, 1995.
30. Ram Charan, "NBR rubber: Its classification and selection criteria," Chennai, 2012.
31. G. Liu, H. Zhang, D. Zhang, H. Zhang, Z. Zhang, X. An and X. Yi, On depression of glass transition temperature of epoxy nanocomposites, J. Mater. Sci., 47 (2012) 6891-6895.
32. A. Hassan, A. Abouel-Kasem, M. A. El-Sharief, F. Yusof, Evaluation of the material constant of nitrile butadiene rubbers (NBRs) with different carbon black loading (CB): FE-simulation and experimental, Polym. 53(17) (2012) 3807-3814
33. A. F. George, The effect of high pressure carbon dioxide on silicone and fluorocarbon seal materials, 10th Int. Conf. on Fluid Seal., Innsbruck, Austria, 1984
34. A. J. Briscoe, S. Zakaria, Interaction of CO2 gas with silicone elastomer at high ambient pressures, J. of Polym. Sci. Part B: Polym. Phys., 29(8) (1991) 989-999
35. G. K. Fleming, W. J. Koros, Dilation of polymers by sorption of carbon dioxide at elevated pressures. 1: Silicone rubber and unconditioned polycarbonate, Macromol. 19(8) (1986) 2285-2291